Electrochimica Acta 366 (2021) 137454

Contents lists available at ScienceDirect

Electrochimica Acta

journal homepage: www.elsevier.com/locate/electacta

Ultrathin clay-containing layer-by-layer separator coating enhances performance of lithium-sulfur batteries

Almagul Mentbayeva[a,b,*], Svetlana Sukhishvili[c], Miras Naizakarayev[a], Nursaule Batyrgali[a], Zhanar Seitzhan[a], Zhumabay Bakenov[a,b]

[a] Department of Chemical and Materials Engineering, School of Engineering and Digital Sciences, National Laboratory Astana, Nazarbayev University, 53 Kabanbay Batyr Avenue, Nur-Sultan 010000, Kazakhstan
[b] Institute of Batteries LLP, 53 Kabanbay Batyr Avenue, Nur-Sultan 010000, Kazakhstan
[c] Department of Materials Science and Engineering, Texas A&M University, 575 Ross St., College Station, TX, United States

ARTICLE INFO

Article history:
Received 25 March 2020
Revised 30 September 2020
Accepted 6 November 2020
Available online 10 November 2020

Keywords:
Lithium-sulfur batteries
Polysulfide shuttle
Halloysite
Layer-by-layer assembly
Lithium dendrite

ABSTRACT

Dissolution of polysulfides upon cycling of the sulfur cathode and their diffusion through the separator membrane – the shuttle effect – is a major factor which deteriorates performance and safety of lithium-sulfur (Li-S) batteries. Here, ultrathin, light-weight polyelectrolyte-clay layer-by-layer assemblies have been developed as versatile nanocoatings on the polypropylene (PP) separator to suppress the shuttle effect. The use of weak polyelectrolytes (polyethyleneimine, PEI, and polyacrylic acid, PAA) and montmorillonite (MMT) or halloysite (Hal) clay nanoparticles enabled full control over mass and charge balance of polyelectrolyte/clay film components, which was critical for achieving ion selectivity and reduction of the polysulfide diffusion. The differences in the geometry and structure of MMT and Hal (nanoplatelets vs. nanotubes), as well as in the pH-controlled charge density of PEI and PAA greatly affected the thickness, morphology, and the ultimate performance of the nanocoatings. In particular, deposition of 450 nm MMT-based coatings at pH 3 and 6 lead to an increase in electrolyte uptake, delayed the lithium dendrite growth and enhanced the discharge capacity of the cell from 300 mAh g^{-1} for bare to 690 mAh g^{-1} for coated PP separator over 200 charge-discharge cycles 0.5 C. At the same time, 250 nm-thick Hal-based coatings deposited at pH 3 resulted in an increase in the Coulombic efficiency from 50% for the bare PP separator to ~99% for the coated one, showing an outstanding performance. Additionally, the polyelectrolyte-clay nanocoatings significantly improve thermal and dimensional stability of the PP separator. The results demonstrate that ultrathin LbL clay-containing coatings on the PP separator membrane can drastically improve the cyclability of the Li-S cells.

1. Introduction

The growing global energy demand [1] generates a need for the development of high-capacity energy storage systems. While currently available rechargeable batteries provide a means for direct, rapid and reversible energy deposition, the cathode materials based on lithium intercalation are limited by theoretical specific capacity and often include low-abundance and toxic metals [2]. As an abundant, cheap and nontoxic material, sulfur presents an attractive alternative for the next-generation battery technologies.

The lithium-sulfur batteries, which were first introduced in 1979 [3], are one of the most promising energy technologies due to their low cost, safety, and high theoretical capacity and energy density [4]. The sulfur cathode has high theoretical capacity and energy density of 1675 mAh g^{-1} and 2600 Wh kg^{-1}, respectively, which are far superior to those of conventional lithium intercalation cathodes (274 mAh g^{-1} and 410 Wh kg^{-1} for graphite/$LiCoO_2$ cells) [5]. However, performance of the Li-S batteries is often impeded by their limited cycle life, low Coulombic efficiency and charge/discharge rate capability [6,7]. These limitations occur due to the back-and-forth diffusion of intermediate redox products, *i.e.* Li_2S_x ($4<x\leq8$) polysulfides, through a separator membrane, known as the shuttle effect [7–10]. Diffusion of polysulfides through the membrane results in reduced reversibility and the Coulombic effi-

* Corresponding author at: School of Engineering and Digital Sciences, National Laboratory Astana, Nazarbayev University, 53 Kabanbay Batyr Avenue, Nur-Sultan 010000, Kazakhstan.
E-mail address: almagul.mentbayeva@nu.edu.kz (A. Mentbayeva).

https://doi.org/10.1016/j.electacta.2020.137454

ciency, as well as the deposition of insoluble Li_2S and Li_2S_2 products on the Li anode, leading to anode passivation.

One strategy explored for preventing the polysulfide shuttle effect involves confining sulfur within porous conductive carbon and polymer matrices [10–12]. While this approach was partially successful in increasing conductivity and mitigating the capacity loss, it also has a drawback of reducing the content of sulfur in the cathode material. Another approach focuses on improving performance of the separator. Coating of a porous PP separator with a layer of various carbon materials was also explored as one approach to block polysulfide diffusion [13,14]. However, weak interactions between carbon materials and polysulfide ions limit the capability of the carbon materials to trap polysulfides during long-term cycling.

The separator is also required to be chemically and mechanically stable under strong reducing/oxidizing conditions and at high temperatures. In addition, the Li dendrite formation and growth during charge/discharge processes also places the Li-S batteries at risk of short-circuit. The main challenge is to engineer a highly stable separator that can support high ionic conductivity of Li ions while selectively rejecting polysulfides and restricting the Li dendrite growth. This challenge has been addressed through surface modifications of the separator in approaches which focus on controlling both wettability of the separator with the electrolyte and its capability to retain electrolyte for good ionic conductivity [15–18]. Along with carbon [13,14], metal oxides [19,20], polymers [21–23] or nanocomposites [24] were used to construct micron-thick coatings using the solution casting technique in order to suppress polysulfide diffusion and improve capacity retention. Among polymers, lithiated Nafion was employed to enhance the cell rate capability [25], improve wettability of the separator by electrolyte [22], and reduce the self-discharge rate of the Li-S cells [26]. However, the solution casting method is not easily controllable, yielding the coatings of variable uniformity and thickness. Moreover, the solution-cast coatings result in a significant increase of the separator thickness and mass, and therefore a decrease in the energy density of the Li-S cell. To overcome this issue, ultrathin, ultralight coatings have been used for surface modification of the separator.

Ultrathin coatings can be deposited on the separator using the layer-by-layer (LbL) technique. The LbL technique yields conformal nanometer-thick coatings on a variety of substrates using environmentally benign aqueous solutions. Moreover, the use of weak polyelectrolytes in LbL assemblies enables controlling the mass and charge ratio of assembled component *via* film assembly conditions [27]. Previously, LbL assembly of weak polyelectrolytes was used to create a separator coating whose excess of negative charge suppressed diffusion of polysulfide anions in the electrochemical cell [28]. However, all-polymer nanocoatings are fundamentally incapable to simultaneously improve the thermal and mechanical stability of the separator.

Here, to our knowledge for the first time, we report construction of nanocomposite clay-polyelectrolyte rather than all-polymer LbL coatings on the separator of the Li-S cell. Specifically, films composed of alternating layers of polyethylene imine (PEI), clay nanoparticles (montmorillonite, MMT, or halloysite, Hal) and poly(acrylic acid) were assembled on the surface of a microporous polypropylene (PP) membrane. Inclusion of clay nanoparticles within the coatings is attractive because of their well-known hydrophilicity, as well as chemical and thermal stability. Previously, LbL assemblies of clay nanoparticles with polyelectrolytes were deposited on other type of non-porous substrates, and demonstrated advanced barrier and flame-retardant properties [29,30]. Clay/polyelectrolyte multilayers have also been explored as water-swellable matrices for controlled retention and release of small molecules in biomedical applications [31]. The only known to us example of the use of clay nanoparticles in Li-S cells demonstrated an improved electrochemical performance achieved with polymer-free MMT coating which were solution-casted on the PP separator [32]. However, the separator mass was doubled as a result of such modification. In contrast to this work, nanocomposite LbL coatings reported here were ultrathin and contained assembled weak polyelectrolytes, whose charge and content, both tunable by the choice of LbL components and assembly conditions, were critical for rejecting polysulfide species. At the same time, the presence of clay nanoparticles in the coatings significantly delayed the growth of lithium dendrites, improved wettability of liquid electrolyte and electrolyte uptake and provided chemical and mechanical stability to the Li-S cell. Importantly, we compare the functionality of the coatings constructed using two different clay nanoparticles – MMT nanoplatelets and Hal nanotubes, which have distinct layered structures of aluminum octahedral and silica tetrahedral sheets with 2:1 and 1:1 ratio, respectively [33–35], and discuss their benefits for improving the electrochemical performance of the Li-S cell. We suggest that the unique hollow tubular structure of Hal with a positive charge on the inner surface created by Al−OH groups, and a negative charge on the outer surface created by Si−O−Si groups plays an important role in polysulfide migration through the coated separator [35]. Also Hal unique nanostructure recently was shown to suppress the polysulfide dissolution via trapping it in the Hal cores within Hal/S composite cathode [36].

2. Experimental section

2.1. Deposition of LbL nanocoatings

Halloysite (Hal) or montmorillonite (MMT) clays (Sigma Aldrich) were stirred and sonicated in deionized (DI) water for 24 h to obtain 2 g dm^{-3} stock solution, which was used to prepare 0.2 g dm^{-3} deposition solutions. Poly(acrylic acid) (PAA) (M_w = 450,000) and branched polyethyleneimine (PEI) (M_w = 750,000, 50 wt% in H_2O, Sigma Aldrich) were diluted with DI water to prepare 0.2 g dm^{-3} polymer solutions.

Polypropylene separators (PP, Celgard 2400) of 25-μm thickness were immersed in a 5% hydrogen peroxide solution for two days prior to LbL deposition. Nanocoatings were then deposited on PP membranes at two different pH of 3 and 6, which are below and near the acidity constant of PAA (pK_a ~ 6) [37], in order to vary the charge density in polyelectrolyte chains. The pH values in all solutions were adjusted to desired values using 1 M HCl and 1 M NaOH. The separator membranes were first immersed in PEI solution for 8 min, rinsed with DI water for 2 min, and then immersed in 0.2 g dm^{-3} solutions of Hal or MMT for 8 min, followed by another rinsing with DI. An additional 8-min immersion in 0.2 g dm^{-3} PAA solution resulted in construction of single trilayer, $(PEI/clay/PAA)_1$. The thicknesses of each layer were measured by ellipsometry and the values are given in the Table S1. The LbL assembly, schematically illustrated in Fig. 1, was repeated *n* times. After deposition of a desired number of trilayers, the separators were dried in a vacuum oven at 45°C for 1 h to remove water accumulated in the membrane pores, and to assure stable performance of the assembled electrochemical cells.

2.2. Material characterization

Field emission scanning electron microscopy (FE-SEM) and transmission electron microscopy images were obtained by using Crossbeam 540, Zeiss and JEOL JEM 1400 plus. SEM with energy-dispersive spectroscopy (EDS) (JSM-IT 200) was used for elemental mapping. Thermal stability of the prepared films was examined by heating of the coated separators in the oven at 90°C, 120°C, and 150°C for 20 min. The Analyzing Digital Images (ADI) software

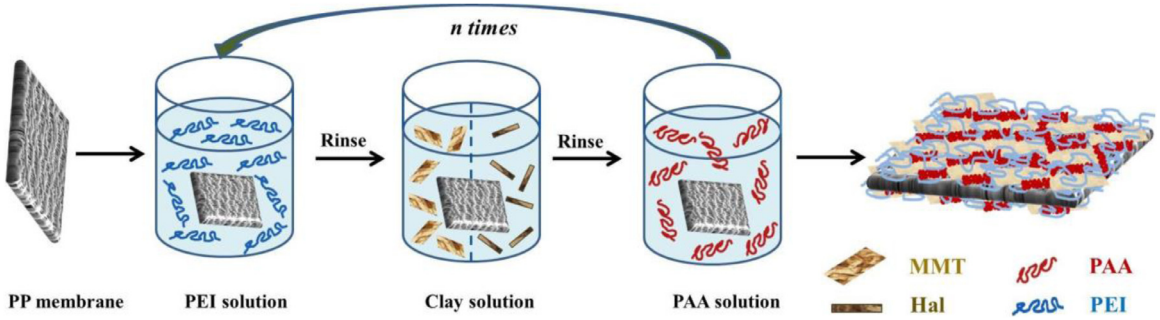

Fig. 1. Schematic representation of LbL assembly on a PP separator.

package was employed to quantify the effect of the thermal treatment on the separator dimensions. The percentage of the separator thermal shrinkage was determined using Eq. (1):

$$Thermal\ shrinkage(\%) = \frac{A - A_0}{A_0} \times 100\% \quad (1)$$

where A_0 is the initial area of a separator of 19 mm in diameter (2.834 cm^2) and A is its area after the heat treatment.

The thickness of the LbL films deposited on the silicon wafers was measured using a PHE-101 Discrete Wavelength Ellipsometer (Angstrom Advanced). Optical properties of the substrates and thickness of the oxide layer were determined prior to film deposition.

For the electrolyte uptake test, the coated and control uncoated separators were wetted in 1 M lithium bis(trifluoromethanesulfonyl) imide (LiTFSI) solution in dioxolane and dimethoxyethane (DOL/DME, 1:1 volume, Sigma Aldrich) for 1 min. Excess amounts of electrolyte droplets accumulated on the film surface was removed by delicate task wipers (KimTech). The liquid electrolyte uptake (wt%) was calculated by Eq. (2):

$$Electrolyte\ uptake(\%) = \frac{W - W_0}{W_0} \times 100\%, \quad (2)$$

where W_0 and W is the weight of the initial and electrolyte-soaked separator, respectively.

Further characterization of the coatings included polysulfide diffusion tests that aimed to demonstrating migration of polysulfides through the coated separators. In a typical experiment, two vials were prepared: a 20 ml vial which was filled with 15 ml of tetrahydrofuran (THF, Sigma Aldrich) and a smaller 3 ml vial which contained 1.5 ml of 1 wt% Li_2S_6 in THF. The separator was inserted within a cap of the smaller vial to cover its 6-mm center opening. The vial was then placed upside down inside a bigger vial which contained THF. Digital images were then taken to record penetration of polysulfides through the separators with time. A 1 wt% Li_2S_6 solution in THF was prepared using stoichiometric amounts of sulfur powder and lithium metal. Li was weighed in a glove box (LABmaster, MBraun Inc.) which was filled with high-purity (99.9995 %) argon gas, and the dry mixture of Li and S was dissolved in THF. The solution was stirred using a magnetic bar for 24 h to ensure complete dissolution of the solids.

The capability of Al_2O_3 nanopowder (Sigma Aldrich), MMT and Hal clays to bind lithium polysulfides was studied using UV-vis spectroscopy. To that end, 1 g of Al_2O_3 nanopowder, MMT or Hal were dried under vacuum at 80 °C overnight and dispersed in 8 ml of THF. This solution was then mixed with a 2 ml of 15 mmol L^{-1} THF solution of polysulfides with the overall atomic composition Li_2S_6, and the mixture was incubated at room temperature for 3 h. The samples were then centrifuged at 600 rpm for 20 min using a Sorvall ST8 centrifuge, and supernatants analyzed using an Evolution 300 UV-vis spectrometer (Thermo Fisher Scientific). Absorbance at 415 nm, characteristic for polysulfide species was used for analysis [38]. The calibration curve (Figure S6) was constructed using mineral-free Li_2S_6 solutions. The quantified amounts of polysulfides adsorbed per gram of Al_2O_3 powder or clay minerals are shown in Fig. S7A. 3 mmol L^{-1} Li_2S_6 solution which did not contain Al_2O_3 or clay was used as a reference solution to calculate the difference in absorption.

2.3. Preparation of sulfur/carbon cathode

Sulfur powder (98%, GOST 127.1, Tengizchevroil, Kazakhstan) and conductive Ketjen black (KB, Ketjen Black International, Japan) were mixed at a weight ratio of 7:3 using ball-milling (PULVERISETTE 7, FRITSCH GmbH). The resulting powder was heated at 280°C for 3 h to facilitate intercalation of sulfur into the porous structure of KB. The resultant S/KB composite contained 66 wt% of sulfur, as was determined by thermogravimetric analysis (TGA). The composite was mixed with acetylene black (AB, MTI, 99.5 % purity) and polyvinylidene fluoride (PVdF, Kynar, HSV900) at a weight ratio of 80:10:10, respectively, and the mixture was dispersed in 1-methyl-2-pyrrolidinone (NMP, Sigma-Aldrich, ≥99.5% purity). The resulting cathode slurry was spread on a conductive carbon-coated aluminum foil (MTI, 20 µm thick) using the doctor blade technique, and dried in a vacuum oven at 60°C for 24 h. In order to ensure good contact between the electrode and the current collector, the cathode was pressed by a roll press. The mass loading of sulfur in the cathode was ~1.5 mg cm^{-2}.

2.4. Electrochemical measurements

The performance of electrochemical cells which were built using the coated separators was examined using coin-type cells (CR2032). The cells typically contained a lithium metal anode (lithium chips of 16 mm in diameter, Hohsen Co., Japan) and a S/KB composite cathode (66 wt% sulfur, 15 mm in diameter), separated by a bare or LbL-coated PP separator (19 mm in diameter). 1 M LiTFSI solution in DOL/DME was used as a liquid electrolyte with the E/S ratio of ~10 µL mg^{-1}. The coin cells were assembled in a glove box filled with a high purity argon gas. All cells were incubated in ambient conditions for at least 5 h prior to electrochemical tests to allow sufficient time for wetting of the separators by the electrolyte. The cells were tested galvanostatically using a multichannel battery tester (BT-2000, Arbin) between 1 and 3 V *vs.* Li^+/Li at a 0.2 C discharge rate (1 C = 1675 mAh g^{-1}).

A multichannel potentiostat/galvanostat (VMP3, Bio-Logic Science Instruments) was utilized to perform cyclic voltammetry (CV) between 1 and 3 V *vs.* Li^+/Li at a scanning rate of 0.1 mV s^{-1}. The electrochemical AC impedance spectroscopy (EIS) measurements were conducted by applying an AC potential of 10 mV over a frequency range between 50 mHz to 1 MHz to determine the effective conductivity of the bare or LbL-coated separators. All measurements were performed using a symmetric Li/Li cell. The effective

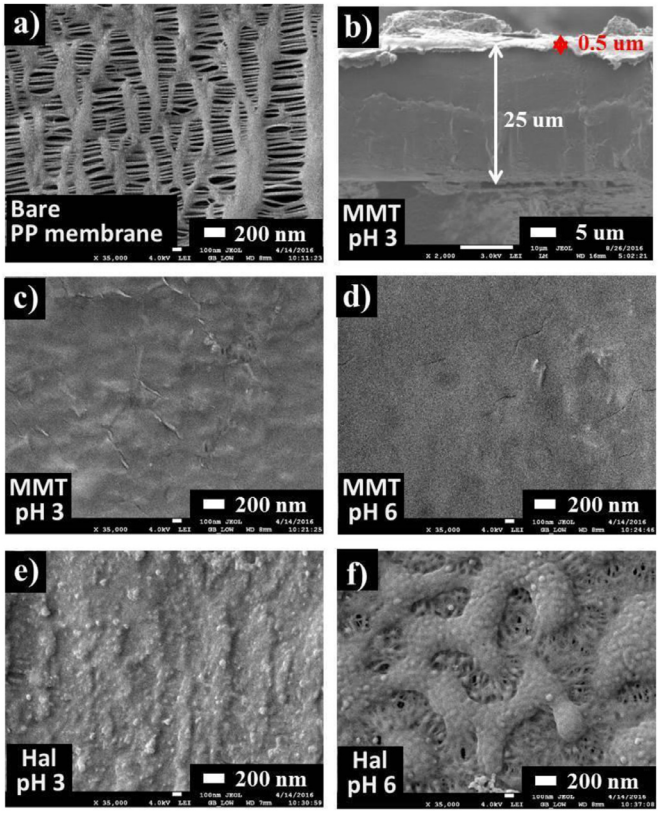

Fig. 2. SEM micrographs of bare (a), and coated PP separators (b–f) modified with $(PEI/MMT/PAA)_5$ films deposited at pH 3 (b and c, b is a cross-sectional view) or 6 (d), as well as with $(PEI/Hal/PAA)_5$ films deposited at pH 3 or 6 (e and f, respectively). In the images, $(PEI/MMT/PAA)_5$ films are abbreviated as MMT, $(PEI/Hal/PAA)_5$ films - as Hal, and pH refers to film assembly conditions.

conductivity σ_{eff} was calculated as follows:

$$\sigma_{eff} = \frac{l}{AR_{el}} \quad (3)$$

where l is thickness of the separator, A is its area, and R_{el} is resistance of the electrolyte.

3. Results and discussion

The major goal of this paper is to explore the capability of ultrathin clay-polyelectrolyte separator coatings to suppress the polysulfide shuttle effect. Prior to electrochemical experiments, the robustness of the coatings was examined using SEM. Fig. S1 reveals that deposition of PEI/clay/PAA LbL coatings on the PP separator required at least five trilayers to uniformly coat the surface. Therefore, all LbL coatings in this study were constructed using five PEI/clay/PAA trilayers. Fig. 2 shows SEM images of bare and LbL-coated microporous PP separators. The bare separator clearly showed ~50–100 nm pores which were homogeneously distributed within the polypropylene matrix, accounting for a 41% porosity [8], which became covered by the deposited clay-containing coatings. The C, O, Si and Al element mapping images of bare and LbL-coated separators with PAA as a top layer confirm the uniform distribution of clay minerals at the surface (Fig. S2). The growth of PEI/clay/PAA trilayer coatings was driven by electrostatic pairing between PEI and PAA, between PAA and positively charged edges of MMT, as well as from the hydrogen bonding between clay and PAA [31,39].

SEM cross-sectional imaging of 5-trilayer PEI/MMT/PAA coatings deposited at pH 3 provided an estimated upper-bound thickness of ~0.5±0.1 μm (Fig. 2b). This estimate is consistent with deposition of a large amount of unprotonated PAA within the film. The growth of the nanocomposite coatings was also followed by ellipsometry when polished silicon wafers were used as a substrate (Fig. S3 and Table S1). The thickness of the first trilayer was 30±10 nm, and increased exponentially with trilayer number for all the systems. The thickness increase associated with each deposited layer of MMT (~22 nm) or Hal (~15 nm) was much higher compared to thickness of PEI (~1.7 nm) and PAA (9±3 nm) layers, as determined by ellipsometry within the first trilayer. These data allowed to estimate the composition of coatings as approximately 70% of MMT (60 % of Hal) and 30–40 % of polymers by volume. Ellipsometric thickness of five-trilayer PEI/MMT/PAA films (420±30 nm) deposited on Si wafers was consistent with that determined by SEM for the coatings deposited on the PP separator. For all polyelectrolyte systems, the separator thickness increased by 500–900 nm after deposition of five-trilayer films to its both sides. Importantly, these thicknesses are considerably smaller than those reported for inorganic coatings (>4 μm) deposited on the separator using the solution casting technique [19,20,22,40].

The deposition of clay-containing coatings dramatically altered the PP separator morphology, with specific changes dependent on clay type and assembly pH (Fig. 2c–2f). It is seen that the use of MMT rather than Hal clay nanoparticles resulted in more homogeneous surface coverage. This can be rationalized by considering drastically different geometries of MMT and Hal nanoparticles (flat and tubular, respectively), which enabled assembly of MMT within continuous films with a “nanobrick wall” architecture composed of stacks of nanoplatelets [41,42]. In contrast, the tubular geometry of Hal inhibited the formation of continuous, homogeneous layers during film assembly.

Importantly, the structure and continuity of nanocomposite coatings were also strongly dependent on pH. While PEI/MMT/PAA coatings assembled at both pH 3 and 6 completely covered the separator, burying its original porous structure, films assembled at pH 3 were more heterogeneous. In particular, ‘bumps’ of a submicron size are seen in Fig. 2c, which most likely are formed by self-aggregated, hydrogen-bonded units of PAA which were largely protonated at pH 3. Interestingly, the use of acidic conditions in a bilayer PEI/MMT system improved rather than deteriorated film ordering [41], suggesting that heterogeneities in Fig. 2c are indeed induced by PAA. Also consistent with this explanation is the fact that more homogeneous films were deposited from solutions at pH 6, where self-aggregation of PAA was suppressed by its enhanced ionization (Fig. 2d). It is also likely that smoothness of the PEI/MMT/PAA films seen at pH 6 resulted from diffusivity of charged PAA chains, as previously suggested for this system [29].

The deposition and morphology of the nanocoatings were even stronger affected by pH in the case of Hal-containing trilayers. Specifically, while PEI/Hal/PAA coatings assembled at pH 3 completely covered the underlying porous PP membrane, films constructed at pH 6 had island-like morphology characteristic of poor adhesion and surface dewetting. It is likely that a decrease in charge density of PEI at pH 6 as compared to pH 3 (pK_a BPEI ~ 6.6) [43] lead to poor coating adhesion to the polypropylene surface, while lack of interactions between Hal and PAA at pH 6 caused irregular coating growth. When films were assembled at a lower pH (pH 3), however, an increased charge density in PEI chains and formation of large interconnected bundles of Hal [44] enabled the formation of a continuous, substrate-adhering films. Obviously, continuity of LbL coatings, along with the film thickness and homogeneity, is expected to improve the barrier properties of the separator to polysulfide diffusion, while incomplete membrane coverage with the coatings should allow polysulfide ions to flow through the separator membrane.

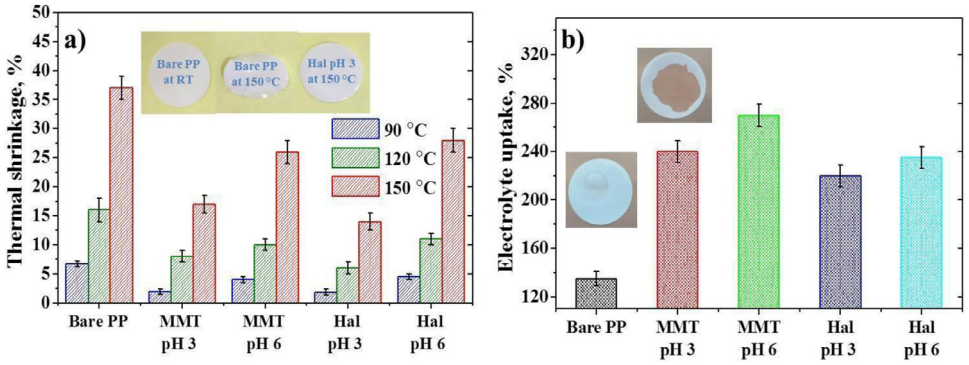

Fig. 3. Thermal dimensional shrinkage (a) and electrolyte uptake (b) of bare and $(PEI/Clay/PAA)_5$-coated PP membrane. In the thermal shrinkage experiments, separate samples of separator membranes were exposed to 90°C, 120°C, or 150°C for 20 min. Abbreviations are the same as in Fig. 2.

3.1. Thermal stability and wettability/permeability of bare and coated separators

One unsolved challenge that impedes the development of batteries with long cycling lifespan is thermal shrinkage of the separators at elevated temperatures and high current densities occurring during battery. Therefore, we aimed to study the effect of the coating deposition on the dimensional stability of the PP membrane at elevated temperatures. The clay components of the films are excellent candidates for improving thermal stability of the separator membranes. Specifically, MMT-containing films were reported to exhibit the flame retardant behavior [30], while halloysite nanotubes were found to preserve their structural integrity up to 1200°C [35]. Fig. 3 shows that while the bare separator exhibited a large, ~37 %, shrinkage when exposed to 150°C for 20 min, all clay-containing LbL coated membranes showed a significantly smaller thermal shrinkage. Furthermore, suppression of the separator shrinkage was highest for $(PEI/clay/PAA)_5$ films assembled at pH 3 rather than 6, with 17 and 14 % shrinkage for the separator coated with MMT- and Hal-containing films, respectively. At the same time, assembly at pH 6 was less efficient in inhibiting the separator shrinkage, with 27% shrinkage for the separator coated with both MMT- and Hal-containing films. The lower efficiency of $(PEI/clay/PAA)_5$ deposited at pH 6 is probably due to more diffuse, softer structure of clay/polyelectrolyte films at pH 6, in which the clay-polyelectrolyte contacts can slide in response to a mechanical force. Moreover, $(PEI/Hal/PAA)_5$ coatings assembled at this pH provided only partial coverage, making the exposed surface of the bare separator vulnerable for thermal damage.

Another important property of a separator is its wettability with electrolyte. Poor absorption of the electrolyte can impair the ionic transport and increase the cell internal resistance, leading to a decrease in ionic conductivity or a direct cell failure. To facilitate absorption of electrolyte and provide long-term electrolyte retention within the separator, hydrophilicity of the intrinsically hydrophobic separator membranes is often increased *via* plasma treatment or surface modification with polymers or inorganic particles [17,18,20,24,45]. Hydrophilic and polar components of LbL coatings were expected to enhance compatibility of the separator with the electrolytes. The electrolyte uptake by the LbL coatings was explored using a 1 M solution of LiTFSI in DOL/DME. Fig. 3b illustrates wettability and electrolyte uptake by the bare and LbL-coated separators. As shown in the inset in Fig. 3b, a droplet of a liquid electrolyte did not spread over the surface of the bare separator, while it wetted the surface of the separator coated with the $(PEI/MMT/PAA)_5$ film. The improved wettability of the coated separators correlated with the enhanced electrolyte uptake. While the electrolyte was not retained by the bare PP separator, all the coated separators retained the electrolyte in the amount of 220–270 wt % of their dry weight. The higher electrolyte uptake by the $(PEI/MMT/PAA)_5$-coated as compared to $(PEI/Hal/PAA)_5$-coated separators (Fig. 3b) are explained by larger thickness of the MMT-containing coatings. Also note that the coatings deposited at a higher pH of 6 showed higher electrolyte uptake, most likely because of the more polar environment within the film created by ionizated PAA.

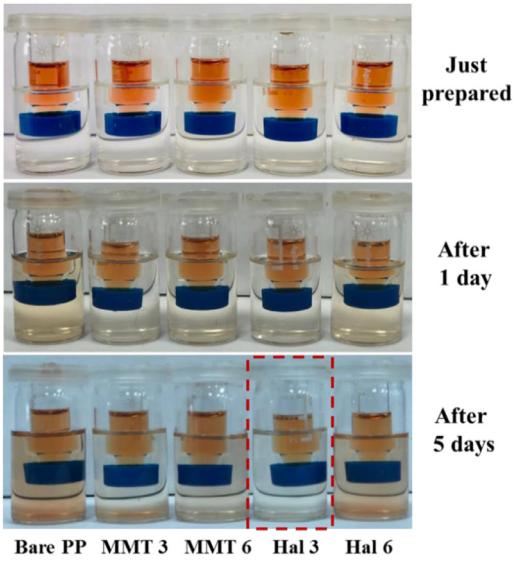

Fig. 4. A polysulfide diffusion experiment which involved the bare and $(PEI/Clay/PAA)_5$-coated PP membranes. The images correspond to 1 min, 1 day and 5 days since the beginning of the experiment. Abbreviations are the same as in Fig. 2.

The capability of the trilayer LbL coatings to serve as a barrier to polysulfide migration was then tested in diffusion experiments which involved 1 wt.% solutions of Li_2S_6 in THF and a two-vial setup shown in Figure S4. The separators were inserted within plastic caps of smaller vials to cover the center opening (see Experimental Section). The dark brown color of Li_2S_6 solutions in the smaller vials enabled visual observation of the transfer of polysulfides through the bare and LbL-modified separators.

As shown in Fig. 4, the polysulfide diffusion was clearly observed after 1 day of the experiment with 1 wt% Li_2S_6 solutions. A lighter color in the receiving THF solution in the case of LbL-coated separators compared to those of the bare separators indicated an improved blocking of the polysulfide diffusion by all four types of the $(PEI/clay/PAA)_5$ coatings. Figure S4 shows that the use of a higher concentrations of Li_2S_6 solutions (*i.e.* 3 wt%) gave similar results. Importantly, despite a larger thickness of the

five-trilayer MMT-containing coatings (~450 nm), the separators with a thinner Hal-containing coating (~250 nm) assembled at pH 3 outperformed other systems, efficiently retaining the inner-vial dark color after 5 days, and showing the lowest permeability to polysulfides at longer times. As expected, however, incomplete membrane coverage by Hal-containing with 5 trilayers assemblies at pH 6 (Fig. 2f) allowed for a considerable flow of polysulfides through the coated separator membranes. The capability of MMT and Hal minerals to adsorb polysulfides was than studied and compared with a reference material – an aluminum oxide (Al_2O_3) nanopowder, which is commonly used as with the cathode or to separator coatings and is known to strongly bind polysulfides and improve the cycling performance of Li-S batteries [20,24,46]. Figure S6 shows that MMT and Hal adsorbed Li_2S_6 more efficiently than control Al_2O_3 powder (3 and 2.7 mg g^{-1} adsorbed amounts, respectively, *vs.* 2.0 mg g^{-1} for Al_2O_3). The difference can result from a larger surface-to volume ratio of nanosized natural clay particles as compared to Al_2O_3 with the particle size of 0.1-0.5 µm. Despite the higher adsorption value for MMT in a powder form, the Hal nanoparticles assembled within LbL films more effectively suppress the transport of polysulfides. One contributing factor can be the more through the more effective tortious diffusion pathway created by Hal nanoparticles: due to their tubular structure, assembled Hal nanoparticles can create more nanoscale domains and thus provide higher tortuosity as compared to stacked MMT nanoparticles. Note that suppression of polysulfide migration by the isolated domains of stacked Hal nanotubes was recently reported for a composite carbon-coated /sulfur cathode of the Li-S batteries [36]. Another contributing factor is the unique charge distribution of Hal nanotubes, i.e. the negatively charged outer shell, and positively charged inner surface [35]. Recent studies show that Hal can be used to improve the lithium ionic conductivity for gel and solid polymer electrolytes [47]. It was suggested that the opposite surface charge on the Hal faces separates lithium salt into lithium ions that absorbed on the outer negatively charged silica surface, and anions that are expected to be adsorbed at the inner, positively charged alumina surface [47]. These characteristics make halloysite nanotubes excellent vehicles for carrying numerous types of cargos, when negatively charged species are sacked into the tube's lumen and positive ones adsorbed on the tube's outer surface [34]. Along with the nanotubular morphology (see TEM data in Figure S7), such distribution creates conditions for cationic perm selectivity [34], when negatively charged polysulfide ions can be selectively trapped within the interior of Hal nanoparticles [36], while small Li^+ ions could permeate through the membrane with minimal diffusional constraints (Fig. 5).

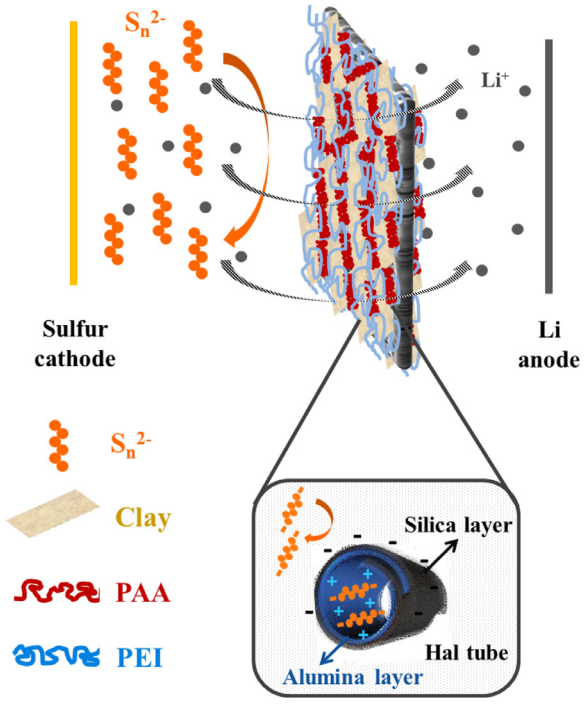

Fig. 5. Illustration of the polysulfide shuttle effect suppression by a (PEI/Clay/PAA)-coated separator.

3.2. Electrochemical studies

Electrochemical studies were then performed with the LbL-coated PP separators. Ionic conductivity of a separator depends on its thickness, porosity/morphology and the capability to uptake a liquid electrolyte. Typically, an increase in the separator thickness and a decrease of its porosity suppress, while an enhanced electrolyte uptake increases ionic conductivity. The overall effect of surface modification on ionic conductivity depends on the relative contributions of the above effects. To explore the effect of clay-containing coatings on the conductivity of the separator to ionic species, electrochemical impedance spectroscopy (EIS) measurements were performed using symmetric Li/separator/Li cells. Figure S8 shows the Nyquist representation of the results for the coated and uncoated separators as plots of negative imaginary part (Z_{im}) *vs.* real part (Z_{re}) of the impedance. These plots were used to determine resistivity (R) from the high-frequency intercepts of the Nyquist plots with the Z_{re} axis, and to calculate ionic conductivity. LbL coating of the separators resulted in an increase in cell resistivity due to an increase in thickness and a decrease in porosity as compared to the bare PP separator. In the case of $(PEI/Hal/PAA)_5$ coatings, the high resistivity of the cell, which was observed in spite of the low coating thickness, offset the positive effect of the enhanced electrolyte uptake by these coatings and resulted in ionic conductivity similar to those observed with the bare separator. In contrast, while $(PEI/MMT/PAA)_5$ coatings were thicker than $(PEI/Hal/PAA)_5$ films, the greatly enhanced electrolyte uptake overpowered the opposing effects of thickness and porosity, leading to a conductivity increase from 0.1703 mS cm^{-1} for the bare separator to 0.1720 and 0.1724 mS cm^{-1} for the separator modified with $(PEI/MMT/PAA)_5$ films deposited at pH 3 and 6, respectively. Select characteristics of bare of the coated separators, such as thickness of the coatings, liquid electrolyte uptake and ionic conductivity are summarized in Table 1.

We then aimed to study the performance of polyelectrolyte-clay coatings in suppressing the growth of lithium dendrites - the major cause the battery failure. To that end, the coated and bare separators were sandwiched in the Li–Li symmetrical cells and charged and discharged at a current density 4 mA cm^{-2} for 1 h of each charge and discharge. As shown in Fig. 6, the cell with bare PP membrane exhibited a stable potential of ~ 200 mV during initial 50 h. After 55 h, however, large fluctuations of the potential from 500 mV to 1100 mV occurred indicating the uncontrolled growth of Li dendrites, which lead to a short circuit and destruction of the separator. In contrast, the cell assembled with LbL-coated separators showed a relatively higher overpotential due to an increased separator thickness and higher resistivity of the cell. The $(PEI/MMT/PAA)_5$ films assembled at pH 3, which had the largest thickness and uniform morphology (see Fig. 2), showed the best performance, preventing growth of Li dendrites for as long as100 h. Hal-containing coatings assembled at pH 3 significantly delayed the cell short circuit to 75 h, while those assembled at pH 6 showed lower suppression of the dendrite growth due to incomplete surface coverage of the separator. The higher Li dendrite suppression ability of MMT-containing coatings might be also related

Table 1
Physical characteristics and properties of bare and coated separators.

	Thickness (μm)	Electrolyte uptake (%)	Ionic conductivity (mS cm^{-1})
PP membrane	25.00±0.01	135±10	0.1703±0.0010
$(PEI/MMT/PAA)_5$ pH 3	25.90±0.05	240±10	0.1720±0.0010
$(PEI/MMT/PAA)_5$ pH 6	25.70±0.05	270±10	0.1724±0.0010
$(PEI/Hal/PAA)_5$ pH 3	25.50±0.05	220±10	0.1697±0.0010
$(PEI/Hal/PAA)_5$ pH 6	25.50±0.05	235±10	0.1704±0.0010

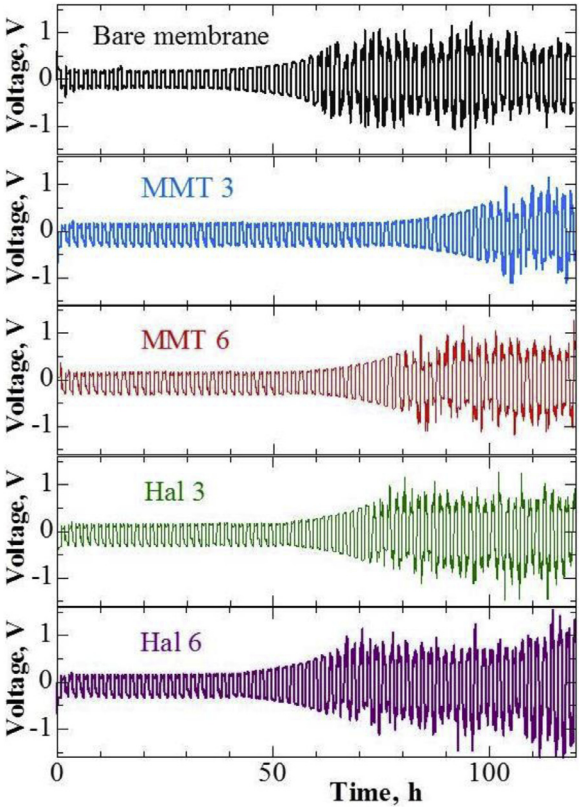

Fig. 6. Galvanostatic cycling voltage profiles for a Li-Li symmetrical coin cells cycled at 4 mA cm^{-2} (4 mAh cm^{-2}) with the bare and $(PEI/Clay/PAA)_5$-coated separators.

to its flat geometry compare to tubular shaped Hal. Recently, a 10 μm thick separator made of highly rigid vermiculite flakes as typical inorganic clay minerals was reported to efficiently prevent the growth of Li dendrite due to mechanical resistance [48]. Nevertheless, this effect is substantial considering 250–450-nm thickness of the coating, which was dramatically lower than several- micron-thick inorganic coatings reported earlier [49]. Moreover, as shown in Fig. S9, the resistance of the separator to the dendrite growth could be further improved by a facile increase in number of deposited PEI/clay/PAA trilayers.

Along with high ionic conductivity, electrochemical stability of the separators is critically important for an efficient and repeatable charge-discharge cycling of the electrochemical cells. The cyclic voltametry (CV) studies enable testing electrochemical stability of the cell components *via* measurements of the reduction-oxidation potentials and detecting unfavorable electrochemical side reactions. Fig. 7 and Figure S10 show CV curves measured in the Li-S coin-type cells with the bare and LbL-coated separators *vs.* Li^+/Li. In these experiments, the cell had a S/KB cathode with 66 wt% of sulfur, a Li anode, and the bare or a $(PEI/Clay/PAA)_5$-coated separator wetted in 1 M LiTFSI in DOL/DME electrolyte. The CV curves for the cells with the bare and LbL-coated separators were almost identical. The two distinct peaks in the cathodic scan are indicative of a two-step reduction of elemental sulfur to the high-order polysulfides S_8^{2-} and S_6^{2-} at ~1.85 V, as well as further reduction to S_2^{2-} and S^{2-} at ~2.25 V [50]. In the subsequent anodic scan, a broad oxidation peak emerged in the 2.6 to 2.9 V range. This peak is associated with conversion of S_2^{2-} and S^{2-} to the high-order polysulfides and elemental sulfur [50]. The absence of any additional peaks in the CV curves for the cell with the LbL-coated separator indicates electrochemical stability of the coatings within the 1-3 V range.

To further explore the effect of LbL coatings on polysulfide diffusion, the cycle performance of the Li-S cells with the bare and coated separators was studied at a 0.2 C rate (1 C = 1675 mAh) as presented in Fig. 8. Fig. 8a-e show a typical charge-discharge profiles of the Li-S cell with two well-defined discharge plateaus at ~2.3 and ~2.0 V [8,9], and one complex charge curve for both the bare and coated separators. A voltage range of charge-discharge plateaus is consistent with the current-voltage data in Fig. 7. The initial discharge capacity of the cell with the bare separator was 915 mAh g^{-1}. The cells with the coated separators yielded an increased initial discharge capacity of ~1200-1300 mAh g^{-1} (Fig. 8b–e). In addition, a lower polarization was observed in the charge-discharge profiles of the cells with coated separators. This positive effect is likely due to the improved hydrophilicity and electrolyte retention of the separators after coating with the clay-containing films.

One of the most important characteristics of the electrochemical cell is its Coulombic efficiency, *i.e.* the ratio of specific discharge to charge capacity. Fig. 8f shows that the cell with the bare separator exhibited a strong overcharge phenomenon resulting in a low Coulombic efficiency of ~50 %, which indicates a significant deterioration of the electrochemical reversibility due to polysulfide shuttle effect. Poor cyclability and low coulombic efficiency are expected for S/KB composite cathode with content of sulfur as high as 66 wt%. This result is easy to understand when considering a highly porous structure of the PP membrane which allowed for facile diffusion of long-chain lithium polysulfides to the anode where they reacted directly with the lithium in a parasitic reaction to generate the lower-order polysulfides. During charge process these species diffused back to the sulfur cathode and oxidized to long-chain polysulfides again which contribute to the overcharge (or self-discharge), resulting in a low Coulombic efficiency [51]. In contrast, all cells with the coated separator showed much higher Coulombic efficiencies. Importantly, the cell with the separator coated with $(PEI/Hal/PAA)_5$ films assembled at pH 3 demonstrated the Coulombic efficiency of 95–99 % (Fig. 8a) which was almost twice higher than that for the cell with the uncoated separator. The greater reversibility of the charge-discharge process resulted in improved cycle performance of the cells with the modified separators (Fig. 8g). The capacity retention at 0.5 C after 200 cycles (45-65 %) was improved by all $(PEI/clay/PAA)_5$ coatings except the one with Hal deposited at pH 6, as compared to the control bare separator (~30 %).

A rate step-progressive test for the cells with the S/KB cathode, and with the bare and coated separators has been carried out as presented in Fig. S11. The cells were galvanostatically cycled at a current density of 0.1 C for 5 cycles, and then the current density was gradually increased up to 2 C. Stable discharge capacities of

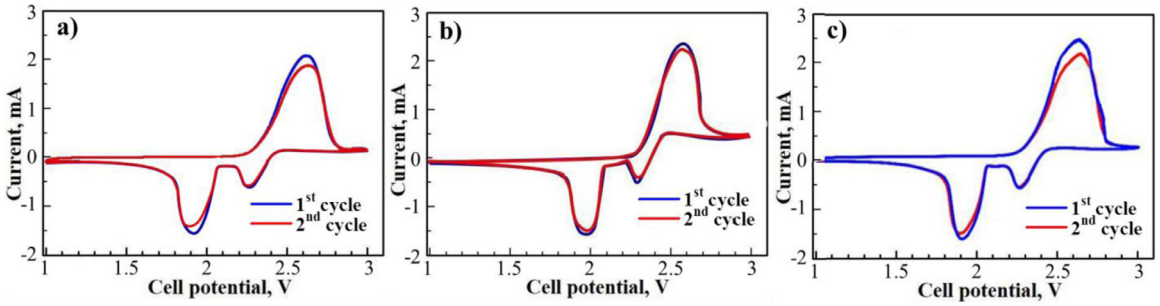

Fig. 7. CV curves for the cells with the bare membrane (a) and the separators coated with $(PEI/MMT/PAA)_5$ (b) and $(PEI/Hal/PAA)_5$ (c) films deposited at pH 3. The scanning rate was 0.1 mV s^{-1}.

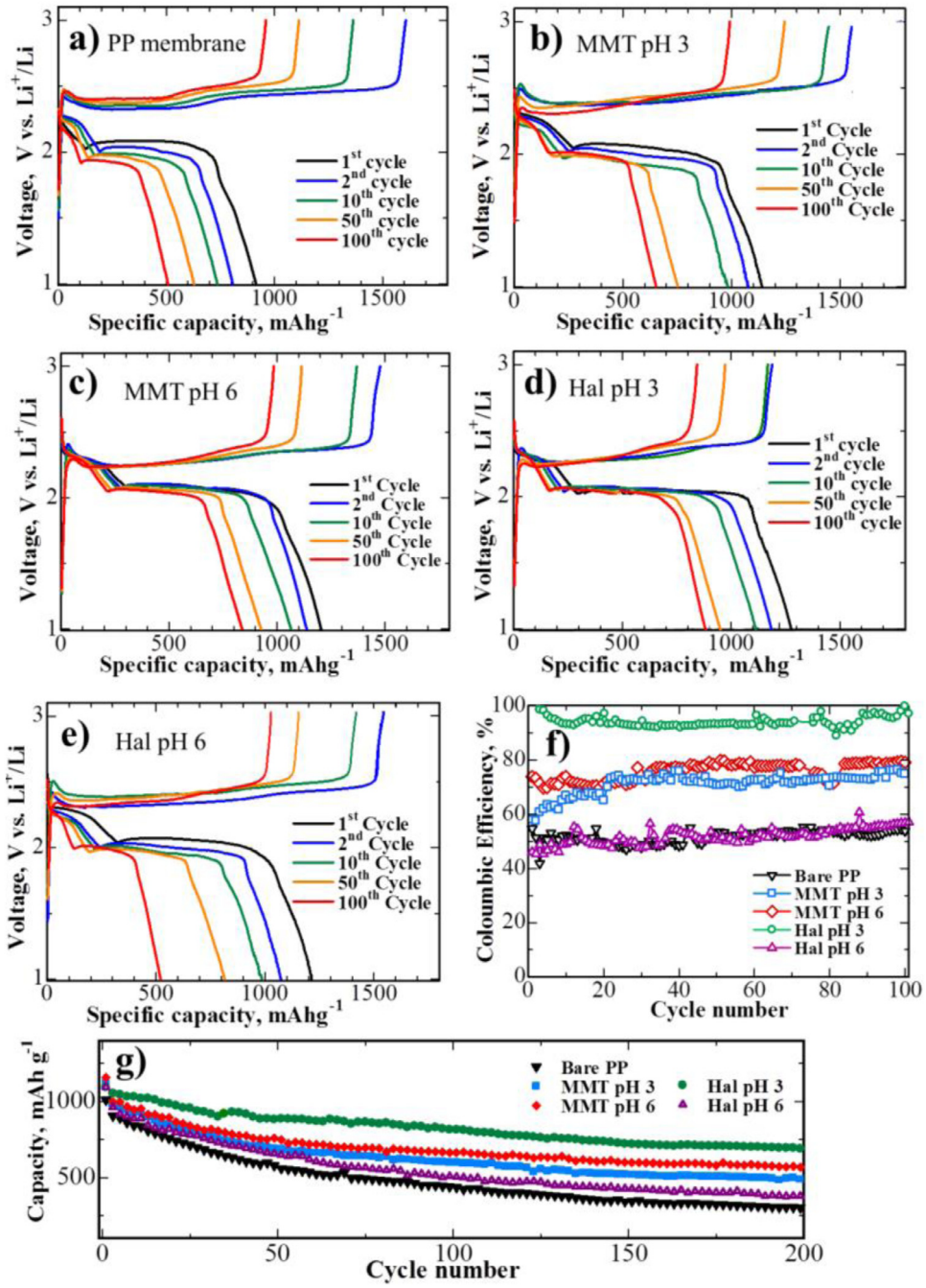

Fig. 8. The charge-discharge profiles at 0.2 C for the Li-S cells with the bare (a) and coated (b–e) PP membrane modified with $(PEI/MMT/PAA)_5$ deposited at pH 3 (b) and 6 (c), or with $(PEI/Hal/PAA)_5$ deposited at pH 3 (d) and 6 (e), as well as Coulombic efficiency *vs.* cycle number (f) and cycle performance for the cells with the bare and coated separators at 0.5 C (g). Abbreviations are the same as in Fig. 2.

1170, 1015, 830, 335 and 90 mAh g^{-1} were obtained for S/KB at the current densities of 0.1, 0.2 C, 0.5 C, 1 C, and 2 C, respectively. The cathode conductivity is a key factor in achieving a high rate performance of Li-S cell. Nevertheless, the $(PEI/Clay/PAA)_5$ coatings at separators slightly improved the C rate performance. 610 and 240 mAh g^{-1} discharge capacities were achieved at 1 C and 2 C, respectively, with the separator coated with $(PEI/Hal/PAA)_5$ films assembled at pH 3, which is due to the increase of the active material utilization at high cycling rates achieved through localization of soluble polysulfides in the cathode side and suppression of their migration.

In order to investigate the morphological stability of the coated separator membranes during cycling, the cell with the separator coated with the Hal-containing nanocoatings were carefully collected from the cell after 100 electrochemical cycles and examined using SEM. Fig. S12 shows that $(PEI/Hal/PAA)_5$ coatings assembled at pH 3 showed no morphological changes on neither side of the separator. The results reveal that the polyelectrolyte-clay trilayer coatings were robust and stable during long-term cycling.

The performance of the separators can also be affected by the thickness of the LbL coatings. Taking the advantage of the LbL technique to precisely control film thickness at the nanoscopic scale, we explored the electrochemical performance of the Li-S cells as a function of trilayer number. Figure S9 b shows the dependence of the Coulombic efficiency of the Li-S cells on trilayer number n for $(PEI/clay/PAA)_n$ films. The Coulombic efficiency of the cells with $(PEI/MMT/PAA)_n$ films deposited at both pH 3 and 6 steadily increased from 50 % to 60-65 % between n=0 and n=5, and continued to increase up to ~80–88 % for n=15. In the case of $(PEI/Hal/PAA)_n$ films deposited at pH 6, the Coulombic efficiency was lower than 65 % up to n=8, which is due to incomplete coverage of membrane's large pores. However, with a further increase in trilayer number (n>10), the Coulombic efficiency increased sharply, reaching 95% for films with n=15. Importantly, with the Hal-containing films deposited at pH 3, the high Coulombic efficiency of ~99 % was achieved after coating with only 5 trilayers, whose deposition resulted in the deposition of ~0.3-μm films on both sides of the separator (Figure S2). At the same time, for $(PEI/MMT/PAA)_n$ films, which had much higher thickness (~0.45 μm for n=5 films deposited on each side, Figure S3), a larger number of trilayers was required to suppress polysulfide diffusion. Nevertheless, comparison of our results with the recently published ones on separator coatings (Table S2) shows that the reported coatings have thickness of several microns, while our coatings are sub-micron-thick. Our optimized sub-micron $(PEI/Clay/PAA)_n$ coatings remarkably improved the cell performance, without a significant addition to the separator's weight and thickness. Along with the type of clay nanoparticle, the film deposition pH played a significant role in the electrochemical performance of Li-S cells with coated separators, which is due to the fact that structure and continuity of nanocomposite coatings were strongly dependent on pH. Therefore, PEI/Hal/PAA coatings deposited at pH 3, which enabled ~99 % Coulombic efficiency using deposition of as few as five trilayers were identified as superior candidates for improving the electrochemical performance of Li-S cells.

4. Conclusion

In summary, we demonstrated that LbL modification of the commercial polypropylene separator with polyelectrolyte-clay trilayer coatings has strongly affected the physico-chemical and electrochemical properties of the coated separator, as well as the ultimate performance of the Li-S cell. The unique structure, geometry and charge of clay nanoparticles (halloysite, Hal *vs* montmorillonite, MMT) programmed the differences in the coating morphology, composition and the ion-conducting properties. The use of weak polyelectrolytes for assembly with clay nanoparticles has provided an additional control of the coating properties *via* adjusting the deposition pH. The clay-polyelectrolyte coatings had substantially improved electrolyte uptake and suppressed thermal shrinkage of the separator, as well as inhibited polysulfide diffusion in the electrochemical cells. Uniform and mechanically durable coatings served as an effective mechanical barrier for lithium dendrites growth and significantly delayed the short circuit failure of the Li/Li symmetric cells. The efficiency of dendrite growth suppression was dependent on the coating thickness and the coating type. Importantly, five-trilayer sub-micron LbL coatings built at pH 3 with Hal nanotubes strongly suppressed the polysulfide shuttle effect, enabling 99% Coulombic efficiency of the lithium-sulfur electrochemical cells. For all the coating types, high Coulombic efficiency could be achieved by increasing number of the deposited trilayers. This work in general demonstrates that surface modification of the polymer separators with clay-containing presents a promising way for improving performance of the Li-S cells.

Declaration of Competing Interest

The authors declare no competing financial interest.

Credit authorship contribution statement

Almagul Mentbayeva: Conceptualization, Methodology, Validation, Data curation, Writing - original draft, Supervision. **Svetlana Sukhishvili:** Data curation, Writing - review & editing. **Miras Naizakarayev:** Validation, Investigation, Visualization. **Nursaule Batyrgali:** Investigation, Resources, Visualization. **Zhanar Seitzhan:** Writing - original draft, Investigation, Resources. **Zhumabay Bakenov:** Writing - review & editing, Project administration, Funding acquisition.

Acknowledgment

This work was supported by the Faculty-development competitive research grant #110119DF4514 "Development of safe and high performance flexible Li-ion batteries" from Nazarbayev University and by the State target program #BR05236524 from the Ministry of Education and Science of the Republic of Kazakhstan. The authors thank Dr. Victor Selin and Mr. Raman Hlushko from Texas A&M University, USA for their help with ellipsometry measurements.

Supplementary materials

Supplementary material associated with this article can be found, in the online version, at doi:10.1016/j.electacta.2020.137454.

References

[1] R. Kumar, J. Liu, J.-Y. Hwang, Y.-K. Sun, Recent research trends in Li–S batteries, J. Mater. Chem. A 6 (2018) 11582–11605, doi:10.1039/C8TA01483C.
[2] J.F. Peters, M. Baumann, B. Zimmermann, J. Braun, M. Weil, The environmental impact of Li-Ion batteries and the role of key parameters–a review, Renew. Susta. Energy Rev. 67 (2017) 491–506, doi:10.1016/j.rser.2016.08.039.
[3] R.D. Rauh, K.M. Abraham, G.F. Pearson, J.K. Surprenant, S.B. Brummer, A lithium/dissolved sulfur battery with an organic electrolyte, J. Electrochem. Soc. 126 (1979) 523–527, doi:10.1149/1.2129079.
[4] Z. Hao, L. Yuan, Z. Li, J. Liu, J. Xiang, C. Wu, R. Zeng, Y. Huang, High performance lithium-sulfur batteries with a facile and effective dual functional separator, Electrochim. Acta 200 (2016) 197–203, doi:10.1016/j.electacta.2016.03.166.
[5] X. Ji, L.F. Nazar, Advances in Li–S batteries, J. Mater. Chem. A 20 (2010) 9821–9826, doi:10.1039/B925751A.
[6] O. Yamamoto, N. Imanishi, Aqueous lithium-air batteries. rechargeable batteries: materials, technologies and new trends, in: Z. Zhang, S.S. Zhang (Eds.), Rechargeable Batteries: Materials, Springer International Publishing, Switzerland, 2015, pp. 559–585. ch. 20.

[7] D. Yang, R. Zhi, D. Ruan, W. Yan, Y. Zhu, Y. Chen, L. Fu, R. Holze, Y. Zhang, Y. Wu, X. Wang, A multifunctional separator for high-performance lithium-sulfur batteries, Electrochim. Acta 334 (2020) 135486, doi:10.1016/j.electacta.2019.135486.

[8] T.B. Reddy, Linden's handbook of batteries, Vol. 4, McGraw-hill, New York, 2011.

[9] H. Peng, X. Wang, Y. Zhao, T. Tan, A. Mentbayeva, Z. Bakenov, Y. Zhang, Enhanced electrochemical performance of sulfur/polyacrylonitrile composite by carbon coating for lithium/sulfur batteries, J. Nanopart. Res. 19 (2017) 348, doi:10.1007/s11051-017-4049-6.

[10] C. Deng, Z. Wang, S. Wang, J. Yu, Inhibition of polysulfide diffusion in lithium–sulfur batteries: mechanism and improvement strategies, J. Mater. Chem. A 7 (2019) 12381–12413, doi:10.1039/C9TA00535H.

[11] S. Kalybekkyzy, A. Mentbayeva, M.V. Kahraman, Y. Zhang, Z. Bakenov, Flexible S/DPAN/KB nanofiber composite as binder-free cathodes for Li-S batteries, J. Electrochem. Soc. 166 (2019) A5396–A5402, doi:10.1149/2.0571903jes.

[12] L. Zhang, Y. Wang, Z. Niu, J. Chen, Advanced nanostructured carbon-based materials for rechargeable lithium-sulfur batteries, Carbon 141 (2019) 400–416, doi:10.1016/j.carbon.2018.09.067.

[13] H. Pan, Z. Tan, H. Zhou, L. Jiang, Z. Huang, Q. Feng, Q. Zhou, S. Ma, Y. Kuang, Fe3C-N-doped carbon modified separator for high performance lithium-sulfur batteries, J. Energy Chem 39 (2019) 101–108, doi:10.1016/j.jechem.2019.01.019.

[14] J. Balach, T. Jaumann, M. Klose, S. Oswald, J. Eckert, L. Giebeler, Functional mesoporous carbon-coated separator for long-life, high-energy lithium–sulfur batteries, Adv. Funct. Mater. 25 (2015) 5285–5291, doi:10.1002/adfm.201502251.

[15] J.Q. Huang, H.J. Peng, X.Y. Liu, W.Z. Qian, F. Wei, Ionic shield for polysulfides towards highly-stable lithium–sulfur batteries, Energy Environ. Sci. 7 (2014) 347–353, doi:10.1039/C3EE42223B.

[16] J.Q. Huang, Q. Zhang, F. Wei, Multi-functional separator/interlayer system for high-stable lithium-sulfur batteries: progress and prospects, Energy Storage Mater 1 (2015) 127–145, doi:10.1016/j.ensm.2015.09.008.

[17] W. Boehnstedt, Separators. Handbook of Battery Materials, C. Daniel, J.O. Besenhard (Eds.), vol. 1, Wiley-VCH Verlag GmbH & Co. KGaA., Weinheim, 2012 Handbook of Battery Materialsch.11, doi:10.1002/ente.201305013.

[18] J. Conder, A. Forner-Cuenca, E. Gubler, L. Gubler, P. Novak, S. Trabesinger, Performance-enhancing asymmetric separator for lithium−sulfur batteries, ACS Appl. Mater. Interf. 8 (2016) 18822–18831, doi:10.1021/acsami.6b04662.

[19] X. Qian, L. Jin, D. Zhao, X. Yang, S. Wang, X. Shen, D. Rao, S. Yao, Y. Zhou, X. Xi, Ketjen black-MnO composite coated separator for high performance rechargeable lithium-sulfur battery, Electrochim. Acta 192 (2016) 346–356, doi:10.1016/j.electacta.2016.01.225.

[20] Z. Zhang, Y. Lai, Z. Zhang, K. Zhang, J. Li, Al_2O_3-coated porous separator for enhanced electrochemical performance of lithium sulfur batteries, Electrochim. Acta 129 (2014) 55–61, doi:10.1016/j.electacta.2014.02.077.

[21] Z. Zhang, Y. Lai, Z. Zhang, K. Zhang, J. Li, Polydopamine-coated separator for high-performance lithium-sulfur batteries, J. Solid State Electr. 19 (2015) 1709–1715, doi:10.1007/s10008-015-2797-8.

[22] M. Rana, M. Li, X. Huang, B. Luo, I. Gentle, R. Knibbe, Recent advances in separators to mitigate technical challenges associated with re-chargeable lithium sulfur batteries, J. Mater. Chem. A 7 (2019) 6596–6615, doi:10.1039/C8TA12066H.

[23] J. Zhu, C. Chen, Y. Lu, J. Zang, M. Jiang, D. Kim, X. Zhang, Highly porous polyacrylonitrile/graphene oxide membrane separator exhibiting excellent anti-self-discharge feature for high-performance lithium–sulfur batteries, Carbon 101 (2016) 272–280, doi:10.1016/j.carbon.2016.02.007.

[24] R. Song, R. Fang, L. Wen, Y. Shi, S. Wang, F. Li, A trilayer separator with dual function for high performance lithium-sulfur batteries, J. Power Sources 301 (2015) 179–186, doi:10.1016/j.jpowsour.2015.10.007.

[25] I. Bauer, S. Thieme, J. Brückner, H. Althues, S. Kaskel, Reduced polysulfide shuttle in lithium-sulfur batteries using Nafion-based separators, J. Power Sources 251 (2014) 417–422, doi:10.1016/j.jpowsour.2013.11.090.

[26] W.-T. Xu, H.-J. Peng, J.-Q. Huang, C.-Z. Zhao, X.-B. Cheng, Q. Zhang, Towards stable lithium–sulfur batteries with a low self-discharge rate: ion diffusion modulation and anode protection, ChemSusChem 8 (2015) 2892–2901, doi:10.1002/cssc.201500428.

[27] G. Decher, J.B. Schlenoff (Eds.), Multilayer Thin Films: Sequential Assembly of Nanocomposite Materials, Wiley-VCH Verlag GmbH & Co. KGaA, Weinheim, 2002.

[28] M. Gu, J. Lee, Y. Kim, J.S. Kim, B. Y.Jang, K.T. Lee, B.-S. Kim, Inhibiting the shuttle effect in lithium–sulfur batteries using a layer-by-layer assembled ion perm selective separator, RSC Adv. 4 (2014) 46940–46946, doi:10.1039/C4RA09718A.

[29] D.A. Hagen, C. Box, S. Greenlee, F. Xiang, O. Regev, J.C. Grunlan, High gas barrier imparted by similarly charged multilayers in Nanobrick wall thin films, RSC Adv. 4 (2014) 18354–18359, doi:10.1039/C4RA01621A.

[30] T. Guin, M. Krecker, A. Milhorn, B. Stevens, J.C. Grunlan, Exceptional flame resistance and gas barrier with thick multilayer Nanobrick wall thin films, Adv. Mater. Interf. 2 (2015) 1500214, doi:10.1002/admi.201500214.

[31] A. Mentbayeva, A. Ospanova, Z. Tashmuhambetova, V. Sokolova, S. Sukhishvili, Polymer−metal complexes in polyelectrolyte multilayer films as catalysts for oxidation of Toluene, Langmuir 28 (2012) 11948–11955, doi:10.1021/la3025342.

[32] W. Ahn, S.N. Lim, D.U. Lee, K.-B. Kim, Z. Chen, S.-H. Yeon, Interaction mechanism between a functionalized protective layer and dissolved polysulfide for extended cycle life of lithium sulfur batteries, J. Mater. Chem. A. 3 (2015) 9461–9467, doi:10.1039/C5TA01378J.

[33] A. Meunier, Clays, Springer-Verlag Berlin Heidelberg, Berlin, 2010.

[34] G. Lazzara, G. Cavallaro, A. Panchal, R. Fakhrullin, A. Stavitskaya, V. Vinokurov, Y. Lvov, An assembly of organic-inorganic composites using halloysite clay nanotubes, Curr. Opin. Colloid Interf. Sci 35 (2018) 42–50, doi:10.1016/j.cocis.2018.01.002.

[35] Y. Lvov, A. Panchal, Y. Fu, R. Fakhrullin, M. Kryuchkova, S. Batasheva, V. Vinokurov, Interfacial self-assembly in halloysite nanotube composites, Langmuir 35 (2019) 8646–8657, doi:10.1021/acs.langmuir.8b04313.

[36] Y. Pei, Y. Wang, Y. Darraf, A.Y. Chang, H. Zhao, X. Liu, J. Liu, Y. Lvov and S. Wang, Confining sulfur particles in clay nanotubes with improved cathode performance of lithium–sulfur batteries. J. Power Sources 450(2020) p. 227698. https://doi.org/10.1016/j.jpowsour.2020.227698.

[37] M. Ling, L. Zhang, T. Zheng, J. Feng, J. Guo, L. Mai, G. Liu, Nucleophilic substitution between polysulfides and binders unexpectedly stabilizing lithium sulfur battery, Nano Energy 38 (2017) 82–90, doi:10.1016/j.nanoen.2017.05.020.

[38] W.S. Tan, R.E. Cohen, M.F. Rubner, S.A. Sukhishvili, Temperature-induced, reversible swelling transitions in multilayers of a cationic triblock copolymer and a polyacid, Macromolecules 43 (2010) 1950–1957, doi:10.1021/ma902459a.

[39] S. Pavlukhina, I. Zhuk, A. Mentbayeva, E. Rautenberg, W. Chang, X. Yu, B. Van De Belt-Gritter, H.J. Busscher, H.C. Van der Mei, S.A. Sukhishvili, Small-molecule-hosting nanocomposite films with multiple bacteria-triggered responses, NPG Asia Mater 6 (2014) e121, doi:10.1038/am.2014.63.

[40] W.-K. Shin, D.-W. Kim, High performance ceramic-coated separators prepared with lithium ion-containing SiO_2 particles for lithium-ion batteries, J. Power Sources 223 (2013) 54–60, doi:10.1016/j.jpowsour.2012.10.082.

[41] D.A. Hagen, L. Saucier, J.C. Grunlan, Controlling effective aspect ratio and packing of clay with pH for improved gas barrier in Nanobrick wall thin films, ACS Appl. Mater. Interf. 6 (2014) 22914–22919, doi:10.1021/am507603z.

[42] P. Podsiadloa, B.S. Shima, N.A. Kotov, Polymer/clay and polymer/carbon nanotube hybrid organic–inorganic multilayered composites made by sequential layering of nanometer scale films, Coord. Chem. Rev. 253 (2009) 2835–2851, doi:10.1016/j.ccr.2009.09.004.

[43] Jin Z, K. Xie, X. Hong, Z. Hu, X. Liu, Application of lithiated Nafion ionomer film as functional separator for lithium sulfur cells, J. Power Sources 218 (2012) 163–167, doi:10.1016/j.jpowsour.2012.06.100.

[44] Y. Joo, Y. Jeon, S.U. Lee, J.H. Sim, J. Ryu, S. Lee, H. Lee, D. Sohn, Aggregation and stabilization of carboxylic acid functionalized halloysite nanotubes (HNT-COOH), J. Phys. Chem. C 116 (2012) 18230–18235, doi:10.1021/jp3038945.

[45] H. Yamin, A. Gorenshtein, J. Penciner, Y. Sternberg, E. Peled, Lithium sulfur battery: oxidation/reduction mechanisms of poly-sulfides in THF solutions, J. Electrochem. Soc. 135 (1988) 1045–1048, doi:10.1149/1.2095868.

[46] D.S. Wu, F. Shi, G. Zhou, C. Zu, C. Liu, K. Liu, Y. Liu, J. Wang, Y. Peng, Y. Cui, Quantitative investigation of polysulfide adsorption capability of candidate materials for Li-S batteries, Energy Storage Mater 13 (2018) 241–246, doi:10.1016/j.ensm.2018.01.020.

[47] Y. Lin, X. Wang, J Liu, J.D Miller, Natural halloysite nano-clay electrolyte for advanced all-solid-state lithium-sulfur batteries, Nano Energy 31 (2017) 478–485, doi:10.1016/j.nanoen.2016.11.045.

[48] R. Xu, Y. Sun, Y. Wang, J. Huang, Q. Zhang, Two-dimensional vermiculite separator for lithium sulfur batteries, Chin Chem Lett. 28 (2017) 2235–2238, doi:10.1016/j.cclet.2017.09.065.

[49] C.Z. Zhao, P.Y. Chen, R. Zhang, X. Chen, B.Q. Li, X.Q. Zhang, X.B. Cheng, Q. Zhang, An ion redistributor for dendrite-free lithium metal anodes, Sci. Adv. 4 (2018) 3446, doi:10.1126/sciadv.aat3446.

[50] C. Barchasz, F. Molton, C. Duboc, J.C. Leprêtre, S. Patoux an, F. Alloin, Lithium/sulfur cell discharge mechanism: an original approach for intermediate species identification, Anal. Chem. 9 (2012) 3973–3980, doi:10.1021/ac2032244.

[51] Y. Diao, K. Xie, S. Xiong, X. Hong, Shuttle phenomenon–the irreversible oxidation mechanism of sulfur active material in Li–S battery, J. Power Sources 235 (2013) 181–186, doi:10.1016/j.jpowsour.2013.01.132.